The Validation of Complete Fourier Direct MR Method for Diffusion MRI via Biological and Numerical Phantoms

Alpay Özcan, *Senior Member, IEEE*, James D. Quirk, Yong Wang, Qing Wang, Peng Sun,
William M. Spees and Sheng–Kwei Song

Abstract—The equations of the Complete Fourier Direct (CFD) MR model are explicitly derived for diffusion weighted NMR experiments. The CFD–MR theory is validated by comparing a biological phantom constructed from nerve bundles and agar gel with its numerical implementation. The displacement integral distribution function estimated from the experimental data is in high agreement with the numerical phantom. CFD–MR's ability to estimate accurately and fully spin diffusion properties demonstrated here, provides the experimental validation of the theoretical CFD–MR model.

I. INTRODUCTION

Aside from elucidating chemical and anatomical properties of biological tissue, Nuclear Magnetic Resonance (NMR) also possesses the ability to report microstructural properties. The capability of diffusion weighted (DW) NMR to describe statistically the motion of spins allows inference of the microstructure they move within.

Historically, Stejskal and Tanner's analysis [1] of the pulsed gradient spin echo sequence (see Fig. 1) constitutes the foundation of the modern diffusion weighted protocols. Therein, DW–NMR signal is modeled by combining the Bloch equations with the diffusion partial differential equation (PDE) with a spatially constant diffusion coefficient. The mathematical foundation of signal formation is investigated in the seminal book by Callaghan [2] by blending PDE and particle method perspectives leading to the derivation of the q–space model. Basically, the q–space methodology establishes a general Fourier relationship between NMR signal attenuation and statistical description of spin motion *via* a probability function that depicts the molecular *displacement* (see [2, Chap. 6]). However, the modeling is based on the narrow–pulse approximation "which can never be realized exactly in a real experiment" as indicated in [2, p. 338]. Later in the book (see [2, Chap. 8]) the methodology is quickly translated to MRI without providing deeper analysis.

One of the important hindrances encountered in the derivation of the q–space model is the utilization of the magnitude of the complex valued free induction decay. Consequently, the properties of Fourier transform always force the q–space analysis to estimate a symmetric probability function. In addition, a symmetric construct also rises up in different non–Fourier approaches inherent to the model infrastructure. For example, diffusion tensor imaging (DTI) [3], [4] intrinsically estimates ellipsoids and high angular resolution diffusion-weighted imaging (HARDI) [5] uses spherical harmonics, which are all symmetric mathematical objects. The only exception is perhaps the generalized DTI (GDTI) model presented in [6] which utilizes skew–symmetric tensors to expand the Fourier operator.

At a deeper level, existing models are founded on physically unsupported mathematical assumptions about the molecular motion in biological tissue, such as the Markovian property. Unlike in a liquid, tissue microstructure makes it impossible to assume that the displacement of the spins at a given time is independent of their past. In tissue, the future motion of the spins is dependent on their current distance from the boundaries and the medium they reside in, so the motion is not Markovian. In fact, it is exactly this dependence that gives to DW methods the ability to infer microstructure. Using particle methods rather than PDEs, all of the issues mentioned above are analyzed, discussed and resolved by the adaptation of the new model, Complete Fourier Direct (CFD) MRI [7], [8]. Therein, it is shown that the signal that comes out of the MRI scanner is the higher dimensional Fourier transform of (joint) distribution function of the number of spins at an initial position and their displacement integral values (rather than the displacements themselves as modeled in the literature). In a sense, the MR scanner acts as a low–pass filter on the displacements [9]. In CFD–MRI the displacement integrals remove the narrow–pulse approximation, and thus, they model the signal in a real experiment. The signal is treated as a complex valued function and therefore does not constrain the distribution function to be symmetric. The CFD–MRI model relies uniquely on the assumption of continuity of the spin motion in biological tissue. The Markovian property is not assumed unlike the diffusion spectrum imaging (DSI) [10]. The distribution function itself is represented 'as it is' i.e. expansions such as spherical harmonics [5], [11] and high order tensors [6], [11] or transforms such as Funk–Radon [12], [10] and diffusion orientation transform [13] or composite sums [14] are not used. The experimental demonstration of the CFD–MRI mathematical model has been accomplished in [8] with an ex–vivo baboon brain. That sample's geometric properties are fairly well known in different regions of the brain but there is obviously no exact description.

Alpay Özcan (corresponding author) is with Mallinckrodt Institute of Radiology, Washington University in Saint Louis, School of Medicine, St. Louis MO 63110, USA. ozcan@zach.wustl.edu

The authors are with Biomedical MR Laboratory, Mallinckrodt Institute of Radiology, Washington University in Saint Louis, School of Medicine, St. Louis MO 63110, USA. jdquirk@wustl.edu, wangyong@wustl.edu, wangqing@wustl.edu, pengsun@bmr.wustl.edu, spees@wustl.edu, ssong@wustl.edu

Here, the DW–NMR experiments are run for two of their advantages. First, as shown in Section II the absence of the imaging gradients facilitates the derivation of the model compared to DW–MRI and the complications originating from them [7], [8] disappear from the experiments. Second, the data set is simpler allowing a reliable interpretation of a simple biological phantom with known properties for a deeper understanding of the method.

In light of all of these observations, this manuscript demonstrates that the CFD–MRI is the unique model that describes DW–MRI signal i.e. the Fourier Transform of the displacement integral distribution. The validation is provided by effectively matching results from the experiments with the biological phantom and the simulations of the numerical phantom.

II. THE DERIVATION OF THE CFD SIGNAL MODEL

In the case of particle methods, the NMR signal is modeled to be originating from the sum of the individual spin magnetizations within the sample. Therefore it is necessary to derive the magnetization of each spin as a function of time and the magnetic field gradients. The evolution of the transverse magnetization of the ith spin is described by a rotating magnetization vector:

$$m_i(t) = e^{-\jmath\,\gamma\,\Omega_i}\,m_i(t_0). \tag{1}$$

Here, γ is the gyromagnetic ratio, the transverse magnetization vector, m_i, is written in complex number form with $m_i(t_0)$ denoting the initial magnetization tipped to the transverse plane at the end of the $\pi/2$ radio frequency (RF) pulse at t_0,

$$\Omega_i(t) = \int_{t_0}^{t} G(x_i, \tau) \cdot x_i(\tau)\,d\tau \tag{2}$$

describes the phase as a function of the magnetic field gradients $G(x,t) \in \mathbb{R}^3$, and the position of the spin $x_i \in \mathbb{R}^3$. Note that the effect of the spin–spin relaxation is neglected assuming that the pulse sequence time is short compared to the relaxation time.

By (1) and (2) the time dependent position of each spin affects the signal. Therefore it must be included in the calculations in the most general fashion:

$$x_i(t) = x_i(t_0) + w_i(t). \tag{3}$$

The function $w_i(t) \in \mathbb{R}^3$ represents the displacement of the spin from its initial position with $w_i(t_0) = 0$, without any assumptions except continuity since a spin cannot disappear at a given point and reappear at another.

The calculations are carried out using the variables defined in Fig. 1 and assuming that the gradient amplifiers are ideal. With the ideal amplifiers, the shape of the gradient pulses treated as rectangular and the evolution of the phase can be described as follows.

In Fig. 1, the $\pi°$ RF pulse between the diffusion gradients, $G_D \in \mathbb{R}^3$, provides theoretical sign reversal of the phase. The
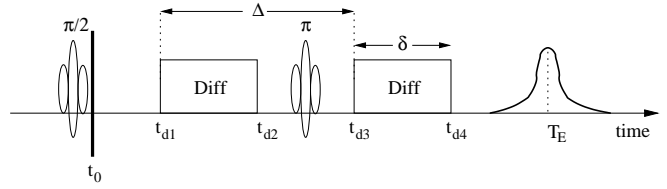

Fig. 1. The Pulsed Gradient Spin–Echo (PGSE) NMR pulse sequence and the definition of the variables used in the calculations. The sampling starts before the echo time T_E to capture the peak value of the free induction decay which is attenuated according to the motion sensitizing magnetic field gradients.

only magnetic field gradients are the motion sensitizing ones and when they are turned on $G(x_i, t) = G_D \cdot x_i(t)$. Therefore, at $t = t_{d4}$, (2) and (3) lead to

$$\Omega_D = \int_{t_{d3}}^{t_{d4}} G_D \cdot x_i(\tau)\,d\tau - \int_{t_{d1}}^{t_{d2}} G_D \cdot x_i(\tau)\,d\tau \tag{4}$$

$$= G_D \cdot \left((t_{d4} - t_{d3})\,x_i(t_0) + \int_{t_{d3}}^{t_{d4}} w_i(\tau)\,d\tau \right)$$

$$- G_D \cdot \left((t_{d2} - t_{d1})\,x_i(t_0) + \int_{t_{d1}}^{t_{d2}} w_i(\tau)\,d\tau \right)$$

$$= G_D \cdot \left(\int_{t_{d3}}^{t_{d4}} w_i(\tau)\,d\tau - \int_{t_{d1}}^{t_{d2}} w_i(\tau)\,d\tau \right)$$

$$+ ((t_{d4} - t_{d3}) - (t_{d2} - t_{d1}))\,G_D \cdot x_i(t_0). \tag{5}$$

The magnetization is given by:

$$m_i(t_{d4}) = e^{-\jmath\,\gamma\,\Omega_D}\,m_i(t_0). \tag{6}$$

If it is so arranged that the diffusion gradient times are equal, $t_{d4} - t_{d3} = t_{d2} - t_{d1} = \delta$, then the last expression is equal to zero in (5). In essence, equal gradient pulse times remove the dependence of the signal on the initial position of each spin. The magnetization is explicitly written as:

$$m_i(t_{d4}) = e^{-\jmath\,\gamma\,G_D \cdot W_i^d}\,m_i(t_0) \tag{7}$$

where

$$W_i^d = \int_{t_{d3}}^{t_{d4}} w_i(\tau)\,d\tau - \int_{t_{d1}}^{t_{d2}} w_i(\tau)\,d\tau \in \mathbb{R}^3 \tag{8}$$

is defined as the displacement integral of the ith spin. This expression is in fact what is being detected with DW–MR.

At any given time, t, the NMR signal originates from the total magnetization:

$$M(t) = \sum_i m_i(t). \tag{9}$$

Specifically for the PGSE sequence, according to (6)–(8), the total magnetization at the echo time T_E is a function of the motion sensitizing magnetic field gradient vector, G_D,

$$M(T_E, G_D) = m_0 \sum_i e^{-\jmath\,\gamma\,G_D \cdot W_i^d} \tag{10}$$

with the initial magnetization, $m_i(t_0) = m_0$, which becomes real valued after an appropriate rotation of the transverse frame if necessary. Equation (10) is just the sum over the (finite) count of spins. At the echo time T_E, $M(G_D)$ can be also calculated in the (continuous) displacement integral space using the distribution function of the displacement integrals, $P_{\text{cfd}}^{\text{nmr}}$:

$$S_{\text{cfd}}^{\text{nmr}} \doteq M(G_D) = \int P_{\text{cfd}}^{\text{nmr}}(W^d) \, e^{-J\gamma \, G_D \cdot W_i^d} \, dW^d, \quad (11)$$

where m_0 is absorbed into $P_{\text{cfd}}^{\text{nmr}}$ for ease of notation. In essence, instead of summing up spin by spin, the signal is obtained in (11) by integrating over the displacement integral space.

The expression of (11) is exactly the Fourier transform of the CFD–NMR distribution function, $P_{\text{cfd}}^{\text{nmr}}$, evaluated at the three dimensional frequency equal to $k_D \doteq G_D$:

$$S_{\text{cfd}}^{\text{nmr}}(k_D) = \mathcal{F}\{P_{\text{cfd}}^{\text{nmr}}\}(k_D). \quad (12)$$

It should be carefully noted that this simple Fourier relationship derived for the NMR experiments is not applicable to the MRI experiments in a straightforward manner. The detailed analysis for MRI carried out in [9], [7], [8] exposes the challenges that arise in the case of imaging.

Since the distribution function $P_{\text{cfd}}^{\text{nmr}}$ is the count of spins, it is real valued. This fact is the only information at hand that guides the estimation of $P_{\text{cfd}}^{\text{nmr}}$ from the DW–MR signal, $S_{\text{cfd}}^{\text{nmr}}$, in (12). In CFD–MR, there are absolutely no other assumptions such as symmetry. Moreover, the distribution function is *not* the transition probability of a stochastic process, therefore it is not tied to the associated properties such as being Markovian.

By the Fourier relationship in (12), the real valued $P_{\text{cfd}}^{\text{nmr}}$ dictates that $S_{\text{cfd}}^{\text{nmr}}$ must be Hermitian symmetric i.e.

$$[S_{\text{cfd}}^{\text{nmr}}(k_D)]^* = S_{\text{cfd}}^{\text{nmr}}(-k_D) \quad (13)$$

where $*$ denotes the complex conjugation.

As a final remark, note that (8) is the key in clarifying the narrow–pulse approximation. The narrow–pulse approximation assumes that the interval of integration is so short that w_i can be treated as a constant during the integration in (8) and the integral can be approximated by:

$$\int_{t_{dk}}^{t_{d(k+1)}} w_i(\tau) \, d\tau = w_i(t_{dk}) \, \delta \quad (14)$$

resulting in

$$W_i^d \simeq (w_i(t_{d(k+2)}) - w_i(t_{dk})) \, \delta, \quad (15)$$

which expresses only the displacement and uses δ as a scale factor for the integration. However, such an approximation is unrealistic even in the simplest case of diffusion in a liquid because the sample paths of Brownian motion are continuous but nowhere differentiable. Therefore the constant value assumption cannot be validated no matter how small the time scale is.

III. Experimental and Numerical Setup

Although the microstructural obstruction of spin motion in biological tissue is reflected in the CFD distribution function, there does not exist an analytical description of $P_{\text{cfd}}^{\text{nmr}}$ even in simple environments. For example, there is no mathematical proof in the literature that when w is Brownian motion, (i.e. with normally distributed independent increments) the distribution function of displacement integrals, W^d, is Gaussian. In regard, the numerical simulations are essential in validating CFD–NMR with biological phantoms of a known microstructure.

The biological phantom investigated in this work consisted of two fixed trigeminal nerves from normal male C57BL/6 mouse (The Jackson Laboratory, Bar Harbor, ME, USA) isolated after fixation. The nerve bundles were placed on each side of a triangular shaped 2% agarose water gel, which provided the set of isotropically diffusing spins (see Fig. 2). The diameter of the nerve bundles varied between 0.5–1 mm along their length. Both bundles were approximately 7 mm long and the agar isosceles straight triangle block had sides of 3.5 mm and thickness equal to 0.5 mm.
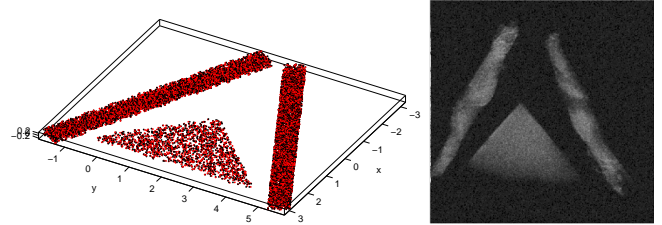

Fig. 2. On the left, the initial (shown in black) and final points (red) of the simulated particles are shown. On the right, the spin–echo MR image of the biological phantom.

The numerical phantom was implemented to mimic the biological phantom as two fiber bundles of length corresponding to 7 mm and containing fibers (mimicking the axons) of diameter $1.25 \, \mu m$ with closed ends. The bundles were oriented by a $53°$ angle with respect to each other and contained 1024 parallel fibers each. The numerical agar gel, which was in the shape of a straight isosceles triangle, had a thickness equal to 0.5 mm and side length equal to 3.5 mm. In each tube 13312 particles and in the agar gel 4000 particles were initially uniformly distributed (see Fig. 2).

The equations (11) and (12) show that DW–NMR provides the Fourier transform of the CFD distribution function, $P_{\text{cfd}}^{\text{nmr}}$, of the spin displacement integrals, W^d. Accordingly, the numerical simulations consisted of

1) calculating the ith spin displacement w_i,
2) evaluating numerically the displacement integral (8),
3) repeating the first two steps for all of the spins and
4) finally computing the distribution of the displacement integral values, $P_{\text{cfd}}^{\text{nmr}}$, in the three dimensional space.

The motion of the particles was simulated using a random walk with normally distributed increments with zero mean. The step size, thus the standard deviation of the increments, was fixed. In the instances when the path crossed the

boundaries, it was readjusted by an elastic collision. There were 3000 steps executed for each of the particles with $\delta_{sim} = 1000$ steps and $\Delta_{sim} = 2000$ steps. This resulted in step time $= \delta/\delta_{sim} = \Delta/\Delta_{sim} = 15 \times 10^{-6}$ s. The step size of the random walk was calculated based on the diffusion coefficient of the water, $s = \sqrt{6 D_{\text{water}} (\text{step time})}$. Free diffusion coefficient for the nerve bundles 2.025×10^{-3} mm^2/s and the diffusion coefficient for the water in agar 1.8×10^{-3} mm^2/s were used [15], yielding respectively to the step sizes $0.427\,\mu$m ($0.64\,\mu$m in the direction of the fibers) and $0.402\,\mu$m. In–house Matlab® (Mathworks, Natick, MA USA) programs were used for all of the computations and to display the graphics and maps.
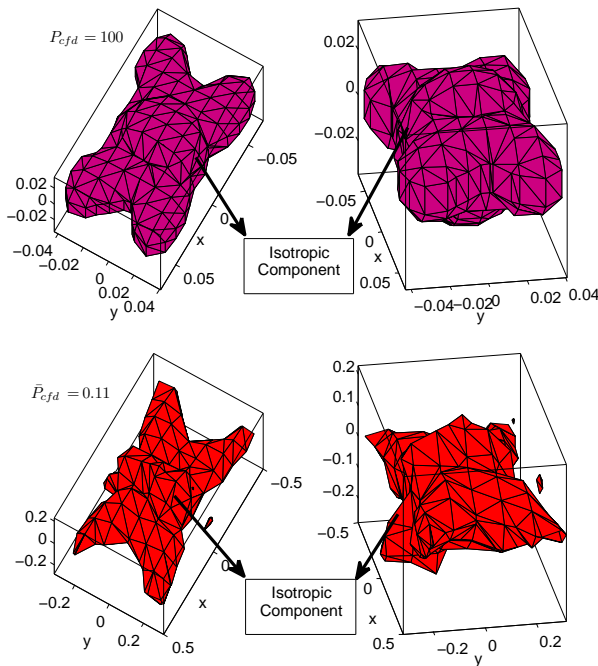

Fig. 3. The isosurfaces of the distribution function of the displacement integrals from numerical (top row) results and the experimental results (bottom row) are shown from two different viewpoints to appreciate the three dimensional structure. The isotropic components, mostly originating from the gel, are located near the origin. The angle between the nerve bundles, $53°$, is apparent in both numerical and experimental results.

The experiments were carried out on a 4.7 Tesla MR scanner (Varian NMR Systems, Palo Alto, CA, USA) with a 12 cm inner diameter gradient system, 60 Gauss/cm maximum gradient strength and 0.27 ms rise time. The repetition time $T_R = 2$ s, echo time $T_E = 60.9$ ms, diffusion pulse time offset $\Delta = 30$ ms and diffusion pulse duration $\delta = 15$ ms were used. The k_D–space was sampled in a uniformly spaced Cartesian grid in a cube $[-45\,\text{G/cm}, 45\,\text{G/cm}]^3$ with $11 \times 11 \times 11$ points, i.e. $\Delta G_D = 9$ G/cm sampling intervals at each dimension resulting in a field of view for the displacement integral space equal to $\pi/(\gamma \Delta G_D) = 0.13048\,\mu$m $\times$ s in each direction. The acquisition time is so arranged that the echo time takes place in the middle of the read–out period. Six sample points from each side of the echo time are averaged to obtain the signal.

IV. CONCLUSION

Note that the measurements only report the displacement integrals which are affected by the relative position of each spin with respect to the nearby microstructure. As long as the relative position of the components of the phantom, e.g. the angle between the nerves, is unchanged, the isosurface will always have the same shape: two crossing cylinders and an ellipsoidal component in the middle corresponding to the isotropic gel sample.

It is clear from Fig. 3 that the angle between the nerves in the experimental $P_{\text{cfd}}^{\text{nmr}}$ isosurface matches the physical phantom as well as the isotropic component. The distribution function estimated from the experimental data is in high agreement with the numerical phantom. CFD–MR's ability to estimate accurately and fully spin diffusion properties, demonstrated here, is unprecedented in the literature. In conclusion, this work provides the experimental validation for the theoretical CFD–MR model.

REFERENCES

[1] E. O. Stejskal and J. Tanner, "Spin diffusion measurements: Spin echoes in the presence of a time-dependent field," *The Journal of Chemical Physics*, vol. 42, no. 1, pp. 288–292, Jan. 1965.

[2] P. T. Callaghan, *Principles of Nuclear Magnetic Resonance Microscopy*. Oxford University Press, 1991.

[3] P. J. Basser, J. Matiello, and D. LeBihan, "Estimation of the effective self-diffusion tensor from the NMR spin echo," *Journal of Magnetic Resonance Series B*, vol. 103, no. 3, pp. 247–254, 1994.

[4] J. Matiello, P. J. Basser, and D. LeBihan, "Analytical expressions for the B matrix in NMR diffusion imaging and spectroscopy," *Journal of Magnetic Resonance Series A*, vol. 108, no. 2, pp. 131–141, 1994.

[5] L. R. Frank, "Anisotropy in high angular resolution diffusion-weighted MRI," *Magnetic Resonance in Medicine*, vol. 45, no. 6, pp. 935–1141, Jun. 2001.

[6] C. Liu, R. Bammer, B. Acar, and M. E. Moseley, "Characterizing non–gaussian diffusion by using generalized diffusion tensors," *Magnetic Resonance in Medicine*, vol. 51, no. 5, pp. 924–937, May 2004.

[7] A. Özcan, "Comparison of the complete fourier direct MRI with existing diffusion weighted MRI methods," in *Proceedings of the 2011 IEEE International Symposium on Biomedical Imaging*, Chicago, Illinois, USA, Apr. 2011, pp. 931–934.

[8] ——, "Complete fourier direct magnetic resonance imaging (CFD–MRI)," *under review*, Apr. 2011.

[9] ——, "A new model for diffusion weighted MRI: Complete fourier direct MRI," in *Proceedings of the 32st Annual International Conference of the IEEE EMB Society*, Buenos Aires, Argentina, Sep. 2010, pp. 2710–2713.

[10] V. J. Wedeen, P. Hagmann, W.-Y. I. Tseng, T. G. Reese, and R. M. Weisskoff, "Mapping complex tissue architecture with diffusion spectrum magnetic resonance imaging," *Magnetic Resonance in Medicine*, vol. 54, no. 6, pp. 1377–1385, Dec. 2005.

[11] E. Özarslan and T. H. Mareci, "Generalized diffusion tensor imaging and analytical relationships between diffusion tensor imaging and high angular resolution diffusion imaging," *Magnetic Resonance in Medicine*, vol. 50, no. 5, pp. 955–965, Nov. 2003.

[12] D. S. Tuch, "Q–ball imaging," *Magnetic Resonance in Medicine*, vol. 52, no. 6, pp. 1358–1372, Nov. 2004.

[13] E. Özarslan, T. M. Shepherd, B. C. Vemuri, S. J. Blackband, and T. H. Mareci, "Resolution of complex tissue microarchitecture using the diffusion orientation transform (DOT)," *NeuroImage*, vol. 31, no. 3, pp. 1086–1103, Jul. 2006.

[14] Y. Assaf and P. Basser, "Composite hindered and restricted model of diffusion (CHARMED) MR imaging of the human brain," *NeuroImage*, vol. 27, no. 1, pp. 48–58, Aug. 2005.

[15] E. Davies, Y. Huang, J. B. Harper, J. M. Hook, D. S. Thomas, I. M. Burgar, and P. J. Lillford, "Dynamics of water in agar gels studied using low and high resolution ^{1}H NMR spectroscopy," *International Journal of Food Science and Technology*, vol. 45, pp. 2502–2507, 2010.